JOURNAL OF MATERIALS SCIENCE 6 (1971) 1277–1285

Inherent Flaw Size and Fracture Energy of Polystyrene

J. MURRAY, D. HULL
Department of Metallurgy and Materials Science, The University of Liverpool, Liverpool, UK

The effect of sharp cracks of various lengths on the fracture behaviour of polystyrene under conditions of constant strain rate and constant load have been investigated. The fracture surfaces can be divided into regions similar in character to those identified on uncracked specimens. The geometry of the crazed fracture surfaces has been studied.

The relation between fracture stress and crack length follows the Griffith equation where the crack length is taken as the total length of the slow crack growth region. The value of fracture energy obtained is compared with that for other grades of polystyrene and other polymers.

In uncracked specimens tested under constant strain-rate and constant load conditions the slow growth region is identified as the inherent flaw. Measurement of the slow growth size allows a calculation of the fracture energy as a function of strain rate or constant load. The fracture energy is found to depend on the shape and dimension of the craze and rate of craze growth.

1. Introduction

The concept of an inherent flaw size in polymers was first introduced by Berry [1-3]. It was found that the fracture stress of polystyrene which contained natural cracks followed a Griffith type variation with crack length. However, for cracks less than 0.17 cm long, fracture did not always occur at the precrack and the fracture stress reached a limiting value. The corresponding crack length a, for an edge crack, was called the inherent flaw size, c_0.

Precracking experiments allow a determination of the fracture surface energy, γ_p, using the Orowan [4] modified Griffith equation

$$\sigma_F = \alpha(E\gamma_p/a)^{\frac{1}{2}} \quad (1)$$

where σ_F is the fracture stress of a specimen containing an edge crack of length a, E is Young's modulus and α is a geometrical constant which takes account of the shape of the crack and the specimen. Berry [2] found γ_p to be 1.7×10^6 ergs cm^{-2} for polystyrene containing edge cracks. Taking σ_F as the fracture stress of uncracked material gives a value of c_0 of 0.11 cm, which is reasonably consistent with the limiting value of a obtained in the precracking experiments.

It is unlikely that the crack length measured by Berry [2] was the true crack length, since no distinction was made between the crack and the craze zone which forms around cracks in polystyrene. Thus, the crack length used included the length of the craze so that the calculated values of γ_p and c_0 will be too high. Another point in Berry's work which requires clarification is the observation that γ_p was not strain rate dependent. The fracture stress of uncracked material is found to be strain rate sensitive, which suggests that the inherent flaw size is not a constant. Since Berry's work many measurements of γ_p in polystyrene have been made (see discussion) which show a wide range of values, with a corresponding variation in c_0.

The inherent flaw concept implies that there is some structural defect which is either pre-existing or is formed prior to fracture. This defect provides a plane of weakness equivalent to a crack of dimension c_0. Kambour [5] proposed that c_0 was a measure of the tendency of a material to craze and Berry [2] suggested that c_0 was the size of the craze in which failure occurred. In general agreement with this, it has been found that in tests over a wide range of strain rates [6] the fracture stress increased

linearly with the logarithm of the strain rate and there was a corresponding decrease in the size of the mirror area. However, in many specimens crazes are obtained which completely cover the specimen cross-section, while retaining a strain rate dependent fracture stress.

In a previous paper [6] we suggested that the slow crack growth region, which was observed to develop in the centre of a craze [7] and to precede fracture, may represent the "inherent flaw". This idea is explored in more detail in this paper to determine the physical significance of c_0. The results reported here supplement those which have been published previously [6, 7] and in interpreting the observations we have had to refer to this data. We have cross-referenced as much as possible to avoid duplication.

2. Experimental Details

Most of the experiments were made on GP Carinex (Shell Chemicals Ltd), $\bar{M}_v = 2.09 \times 10^5$, which had been compression moulded into sheet 3 mm thick as described previously [7]. Additional experiments were made using SB 59 Carinex, $\bar{M}_v = 1.73 \times 10^5$, compression moulded into sheet at a pressure of 1 kg mm^{-2} at 460° K and slow cooled, and HR Carinex, $\bar{M}_v = 2.03 \times 10^5$, which was hot milled before compression moulding as above. Both GP and SB 59 Carinex contain preparations of mineral oil to act as a lubricant and SB 59 is designated as an improved general purpose grade. HR Carinex contains no additions of lubricant.

The tensile specimens were cut from the compression moulded sheet; two different shapes being used. The first was identical to that described previously [7] and the second had parallel sides. Artificial cracks were introduced into the parallel sided specimens by pressing a sharp wedge into the faces of a fine saw cut [1]. The saw cut was subsequently removed and control of the crack length was obtained by grinding the edge of the specimen on emery paper.

All the tensile tests were made on an Instron machine. Both constant strain rate and constant load tests were used and the methods are given in [6]. The precracked specimens were tested either at a fixed strain rate of 10^{-4} sec^{-1} or at constant load. For the latter the initial load was achieved by raising the stress using a strain rate of 10^{-4} sec^{-1}; the load was maintained constant to within $\pm 1\%$ by cycling the load in the Instron machine between two close limits.

The fracture surfaces were studied using optical microscopy and interferometric techniques.

3. Experimental Observations

3.1. Fracture Surfaces

Tensile tests on initially uncracked material confirm the previous observations [6-9] and indicate that the fracture surface may be divided up into three main regions. Region A is an area of slow crack propagation which contains the origin of fracture. Region B is an area where the crack propagates rapidly through a primary craze. Region C is an area of fast crack propagation in which new crazes form rapidly at the tip of the moving crack. In HR Carinex tested at a strain rate of 10^{-4} sec^{-1} primary crazes develop across the whole of the specimen cross-section before final fracture and Region C is absent.

The appearance of the fracture surface of precracked specimens is entirely consistent with the observations summarised above. A typical fracture surface is shown in fig. 1a and the schematic diagram fig. 1b illustrates some of the details associated with the fracture process. The formation of the precrack involves wedging open a saw cut slot. This produces a slowly propagating crack analogous to Region A; the crack propagates through a large craze which grows as the crack grows. The boundary of the precrack is pp′ in fig. 1 and the extent of the craze ahead of the precrack is qq′. When the precracked specimen is tested in tension the precrack grows slowly through the original craze zone which continues to grow ahead of the crack. At some critical stage defined by rr′ on the fracture surface the crack starts to propagate along the craze matrix interface, analogous to Region B, and the boundary ss′ marks the extent of crack propagation through primary craze. The boundary ss′ outlines the "mirror" region of fracture and the beginning of Region C.

Precracked specimens of SB 59 showed similar features to GP Carinex except that the slow growth region between qq′ and rr′ was much smaller.

3.2. Distribution of Craze around the Crack

The geometry of crazes around precracks was examined in sections parallel to the plane of the sheet specimens and also on the fracture surfaces. The crazes around cracks in GP and SB 59 Carinex were identical and their shape corresponded to those described by Van den

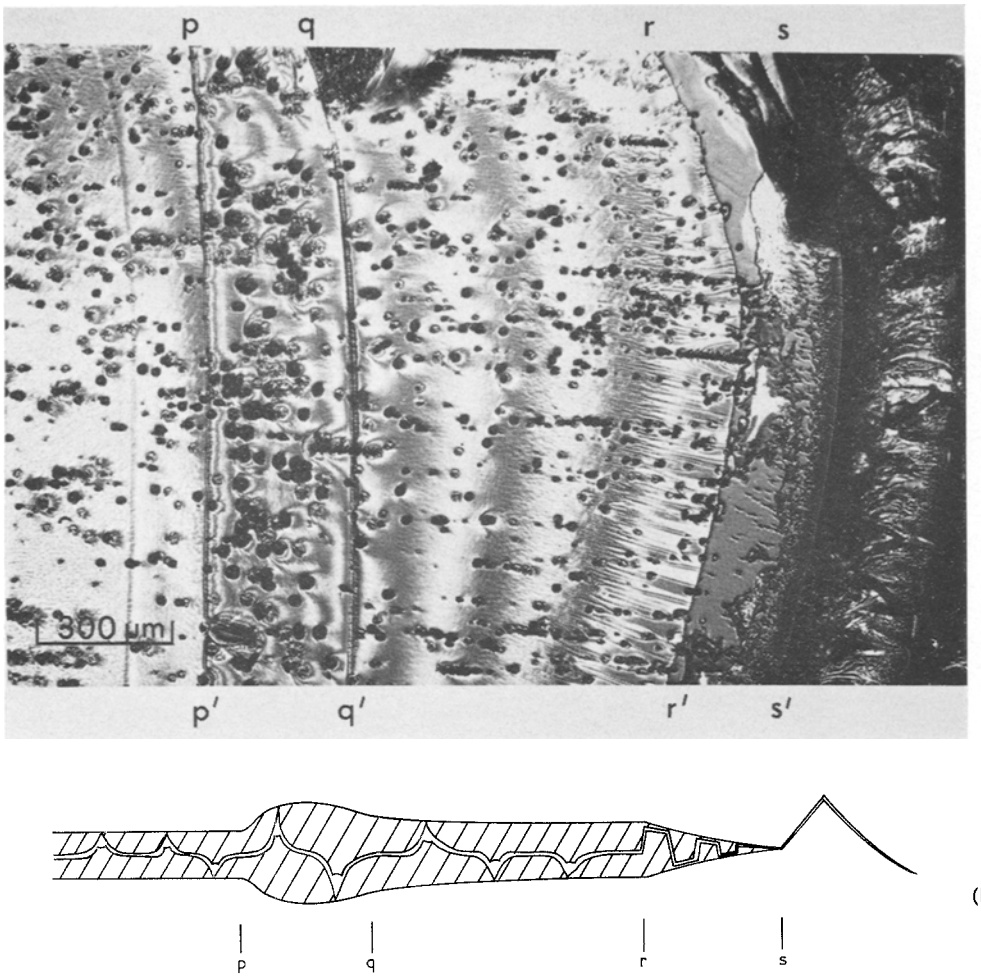

Figure 1 (a) Typical fracture surface of a precracked specimen of GP Carinex. The tip of the precrack is at pp′ and the tip of the pre-existing craze at qq′. The crack and craze have grown slowly in the direction left-right up to the boundary rr′ and there are many secondary fracture features. The crack has then propagated rapidly through the craze zone to ss′ and beyond this has generated a different type of craze field. (b) Schematic diagram (not to scale) of a section through the fracture surface of the specimen in fig. 1a showing the craze geometry and characteristics of crack propagation.

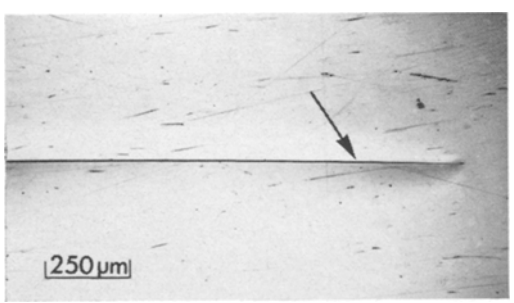

Figure 2 Reflected light micrograph of a crack and craze at the surface of an SB 59 Carinex specimen. The specimen is unstressed and hence the crack tip cannot be seen; its position is marked by an arrow.

Boogaart [10] and Kambour [5] for cracks in polymethylmethacrylate. This shape was also deduced in our previous work [11] on polystyrene from fracture surface observations and direct examination of cracks during growth. An example of the craze formed around a crack is shown in fig. 2. In the slow crack propagation region the craze consists of a uniform layer on each fracture face and the thickness of this layer may be deduced [6] from measurements of the depth of the secondary fracture features (parabolas) on the fracture surface. In fig. 1 the thickness of the craze varies along the length of the crack and it is found that the thickness is

dependent on the conditions of crack propagation. Thus, the parabolas in the band between pp′ and qq′ are considerably deeper than in the other regions. Typical profiles of the thickness variation of the crazed volume around the crack are shown in figs. 3 and 4 for constant load and constant strain rate tests. In fig. 3 the three

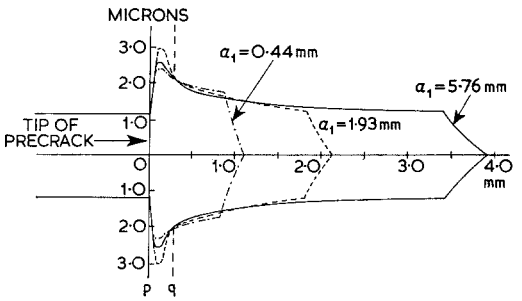

Figure 3 Variation of craze thickness with distance along the fracture surface of several precracked specimens tested under constant load conditions. The horizontal axis represents the fracture plane. (Note the difference in scales on the two axes.)

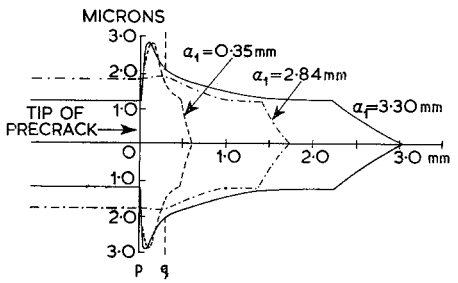

Figure 4 Variation of craze thickness with distance along the fracture surface of several precracked specimens tested under constant strain rate conditions.

curves correspond to different loads and different initial crack lengths, but they all have the same form. The thickness of the craze associated with the precrack is constant and there is a region of thick craze in the zone pp′ – qq′. As the crack propagates slowly within the craze, in zone qq′ – rr′, the total craze thickness reaches a constant value of about 2.5 μm before the onset of Region B in the zone rr′ – ss′. The shapes in fig. 4 have the same general form except that for crack length a_1 = 2.84 mm the craze does not show the pronounced thickening in zone pp′ – qq′. In this specimen, unlike all the others, the precrack was introduced while the specimen was under tensile load in the Instron machine and was immediately tested without unloading. Thus,

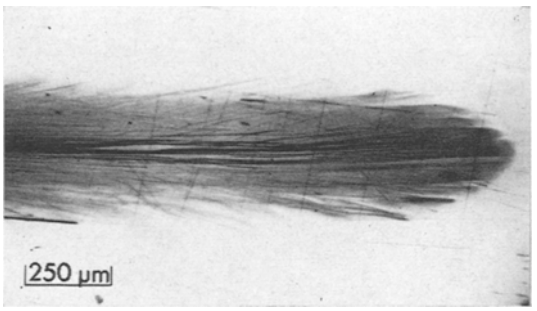

Figure 5 Reflected light micrograph of an unstressed crack and crazes in HR Carinex. The shadow region is due to a bundle of crazes around the crack tip, cf. fig. 2.

the thickening in zone pp′ – qq′ may be attributed to the initial cycle of loading and unloading during precracking of the specimen.

In HR Carinex fine bundles of crazes formed around the precrack, fig. 5, and were similar to those reported by Berry [2].

3.3 Effect of Crack Length on Fracture Stress

The length of the crack at different stages of fracture may be defined by the dimensions: a_1, the length of the original precrack indicated by the region up to the boundary pp′ on the fracture surface (fig. 1); a_2, the total length of the crack which has propagated through a craze indicated by the region up to rr′, and M the dimensions of the mirror area of fracture given by the region up to ss′. The values of a_1, a_2 and M for constant load and constant strain rate tests on GP Carinex are given in tables I and II respectively, along with the corresponding fracture stresses. A few values for SB 59 Carinex tested at constant strain rate are given in table III.

In the discussion it is suggested that a_2 is the most meaningful crack length parameter to substitute in the Griffith equation for calculating fracture energies. Accordingly, a_2 has been plotted against fracture stress in fig. 6 for GP Carinex. The curves correspond to the best fit for a Griffith type variation of a_2 with σ_F. Taking α in equation 1 as $(2E/1-\nu^2)^{\frac{1}{2}}$ where $E = 2.7 \times 10^{10}$ dynes cm^{-2} and $\nu = 0.33$ gives $\gamma_p = 2.3 \pm 0.4 \times 10^5$ and $2.9 \pm 0.7 \times 10^5$ ergs cm^{-2} for constant load and constant strain rate respectively for the curves in fig. 6 and the data in tables I and II. The value of γ_p using the data in table III for SB 59 Carinex is $1.5 \pm 0.5 \times 10^5$ ergs cm^{-2}

3.4. Observations on Uncracked Specimens

In a previous paper [6] the appearance of the

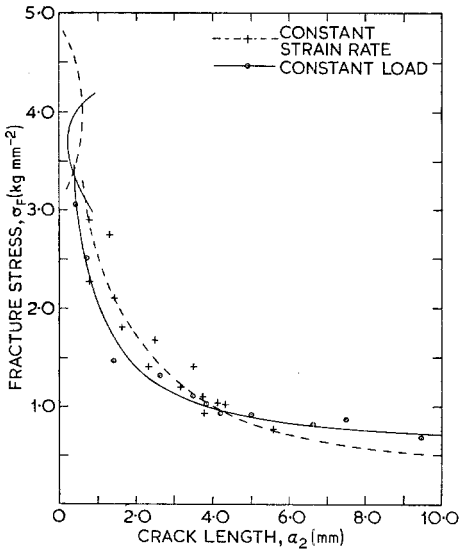

Figure 6 Variation of fracture stress with slow crack length for precracked specimens of GP Carinex tested under conditions of constant strain rate (10^{-4} sec^{-2}) and constant load. The graph also includes data shown in fig. 8 obtained from uncracked specimens at various constant strain rates and constant loads, which are included without the experimental points.

TABLE I Variation of fracture stress σ_F, with pre-introduced crack length a_1 for constant load tests on GP Carinex. The total slow growth size is denoted by a_2, the mirror size by M and the time to break by t_b.

σ_F kg mm^{-2}	a_1 mm	a_2 mm	M mm	t_b sec
3.10	0*	0.27	3.00	1.21×10^4
2.54	0.44	0.80	1.22	3.98×10^4
1.46	0.76	1.61	1.89	1.07×10^4
1.35	1.54	2.70	2.92	1.25×10^3
1.10	1.79	3.46	3.71	7.79×10^2
1.00	1.93	3.75	3.99	5.64×10^2
0.92	2.32	4.17	4.42	2.53×10^3
0.91	2.82	5.13	5.38	1.77×10^2
0.90	3.88	7.36	7.74	3.84×10
0.79	3.81	6.71	7.02	2.61×10^4
0.72	5.76	9.40	9.66	2.06×10^2

fracture surface, the morphology of the craze and details of fracture stresses for GP Carinex have been described. The specimens which were tested in this previous work have been further examined to determine the dimensions of the slow crack growth region, c, and the size of the mirror area, M. As reported, reference [6], the position of the slow growth region within the mirror area varied with strain rate, and this made it difficult

TABLE II Variation of fracture stress σ_F, with pre-introduced crack length a_1 for constant strain rate tests (10^{-4} sec^{-1}) on GP Carinex. The total slow growth size is denoted by a_2, and the mirror size by M.

σ_F kg mm^{-2}	a_1 mm	a_2 mm	M mm
2.89	0.36	0.89	1.45
2.72	0.33	1.16	1.49
2.31	0.35	0.93	1.24
2.11	0.72	1.62	1.89
1.83	1.06	1.59	1.87
1.69	1.55	2.49	2.63
1.41	2.49	3.40	3.44
1.40	1.32	2.27	2.52
1.21	2.64	6.13	6.87
1.20	1.59	3.02	3.49
1.10	2.71	3.63	3.85
1.05	3.31	4.01	4.28
0.99	2.84	4.25	4.48
0.88	3.26	3.75	4.04
0.77	4.55	5.50	5.77

TABLE III Variation of fracture stress σ_F with pre-introduced crack length a_1 for constant strain rate tests (10^{-4} sec^{-1}) on SB59 Carinex. The total slow growth size is denoted by a_2 and the mirror size by M.

σ_F kg mm^{-2}	a_1 mm	a_2 mm	M mm
3.28	0.15	0.31	1.14
1.61	1.25	1.45	1.84
1.47	1.01	1.04	1.41
1.44	1.07	1.18	1.62
1.07	1.10	1.30	1.79
0.94	2.85	2.93	3.39
0.86	3.03	3.07	3.44
0.70	4.47	4.60	5.08

to measure the crack and mirror dimensions in exactly the same way in each specimen. The dimensions which were measured are indicated in fig. 7 and the variations of c and M with σ_F are shown in fig. 8.

4. Discussion

The observations on fracture in precracked and uncracked specimens indicate that, apart from the nucleation process, the processes associated with the development and growth of a crack in a craze are identical. Three main steps have been identified.

(i) A large thick craze grows under the influence of the tensile stress. In cracked specimens the craze forms and grows at the tip of the precrack and in

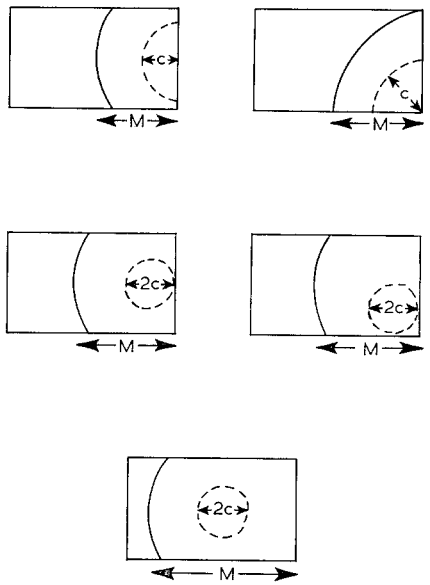

Figure 7 Diagrammatic representation showing the various positions of the slow growth region on the fracture surface. The dimensions M and c are shown.

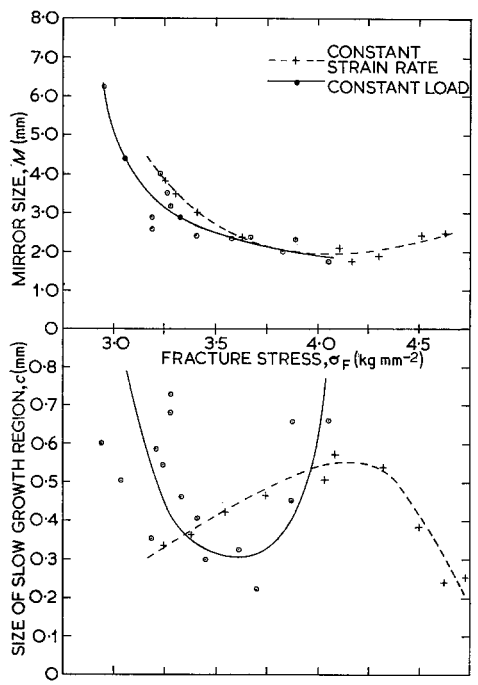

Figure 8 Variation of the size of the mirror region and the slow growth region with fracture stress under conditions of constant strain rate and constant load.

uncracked specimens at some local stress concentration.

(ii) Slow crack growth occurs within the craze; the crack gradually increasing in speed with the craze growing ahead of it.

(iii) At a critical stage the mechanism of crack growth changes to produce the fragmented craze film in Region B.

The most easily defined dimensions on the fracture surfaces are M, c and a_2. The change in fracture mode referred to in (iii) above occurs at crack lengths of c and a_2 for uncracked and precracked specimens respectively, and corresponds to an instability in the sense that once these dimensions are exceeded it appears that crack propagation becomes catastrophic. Since the same instability occurred in both types of specimen it should be possible to correlate the two sets of results. The work of Williams and co-workers [12, 13] has shown that the fracture toughness, and hence γ_p, of thermoplastics varies with crack velocity. For the purpose of this discussion it is assumed that the instability in crack growth occurs at a constant crack velocity irrespective of the type of test.

The values of γ_p of 2.3 and 2.9 $\times$ 10^5 ergs cm^{-2} obtained in these experiments for GP Carinex under different test conditions are considerably lower than most of the previous results for polystyrene, but they are comparable to the fracture energies observed in PMMA (see table IV). The craze around cracks which propagate with these low energies forms a as single narrow zone in the same plane as the crack. The slightly lower value of γ_p of 1.5 $\times$ 10^5 ergs cm^{-2} was observed in SB 59 Carinex. The wide variation in the published values of γ_p is undoubtedly due to the different grades of polystyrene used which result in different distributions of craze ahead of the crack. Thus, HR Carinex develops large bundles of crazes around the tip of the crack and the fracture energy is correspondingly higher. This may be attributed to a reduction of the stress intensity at the crack tip due to craze formation, or alternatively to the energy expended in deforming and propagating the bundle of crazes. Similar observations have been made recently by Williams [22]. In tapered cleavage specimens he obtained fracture toughness values similar to those reported by Berry [2]. However, when a crack was initiated by high frequency fatigue further crack extension occurred without producing a bundle of crazes at the crack tip and the fracture toughness was similar to the results reported in this work.

Following Berry [2], a computation of c_0 for uncracked specimens can be made by substitu-

TABLE IV Fracture energies measured on various types of PMMA and polystyrene using the indicated testing methods.

Material	Method	$\gamma_p \times 10^{-5}$ ergs cm^{-2}	Ref.
PMMA, Perspex (I.C.I)	Edge crack cleavage (slow propagation)	4.9	[14]
	Edge crack cleavage (fast propagation)	3.5	[14]
	Central cleavage crack	4.2	[15]
		5.3	[16]
PMMA Plexiglass II (Rohm & Haas)	Tensile precrack	2.1	[1]
	Cleavage, grooved	1.4	[17]
		1.2	[18]
PMMA, unspecified	Stable tensile crack propagation	1.6	[10]
PMMA Acrylite (Mitsubishi Rayon Inc.)	Tensile precrack	3.6	[19]
PMMA Perspex (I.C.I)	Three point bending	6.5	[20]
	Compliance analysis	5.5	[20]
	Area under stress strain curve	3.0	[20]
	Impact, three point notch bending	3.5	[12]
	Cleavage:		
	Crack velocity $< 10^{-6}$ in sec^{-1}	2.6	[13]
	Crack velocity —1 in sec^{-1}	6.9	[13]
Polystyrene, Styron (Dow)	Edge crack cleavage	2.5	[14]
	Central cleavage crack	8.8	[16]
Polystyrene, Lustrex	Central cleavage crack (slow propagation)	34	[16]
	Central cleavage crack (fast propagation)	9.8	[16]
Polystyrene (unspecified)	Tensile precrack	17	[2]
Polystyrene Styron (Dow)	Cleavage, grooved	7.1	[17]
Polystyrene Styron (Dow)		4.0	[18]
Polystyrene (unspecified)	Controlled propagation, three point bending	10	[21]
Polystyrene (unspecified)	Double edge notch	7	[12]

tion into equation 1. Using the values of γ_p and σ_F determined at a constant strain rate of 10^{-4} sec^{-1} gives

(*a*) GP; $c_0 = 0.035$ cm

(*b*) SB 59; $c_0 = 0.017$ cm

Pre-existing flaws of this size would be readily visible and the specimen preparation techniques used in this work ensure that they are not present. It follows that the flaws must be generated during testing by dynamic processes such as those associated with crazing.

Measurements of the mirror area (i.e. region A + region B) indicated that this increased in size as the strain rate or constant applied load decreased, see fig. 8. If the mirror surface represents the inherent flaw size this variation is broadly consistent with the Griffith theory, i.e. for a constant γ_p an increase in c_0 results in a decrease in σ_F. However, the mirror sizes for a strain rate of 10^{-4} sec^{-1} are about 0.2 cm for both SB 59 and GP Carinex. These values are in poor agreement with the calculated flaw sizes. The size of the slow growth regions for the same strain rate are

(*a*) GP ; 0.053 ± 0.01 cm

(*b*) SB 59; 0.013 ± 0.002 cm

These values are in reasonable agreement with the calculated c_0 values quoted above, and suggest that the slow growth size is equivalent to the inherent flaw size.

The measured slow growth sizes plotted in fig. 8 have been used in fig. 6 to extend the range to shorter crack lengths. The results from uncracked specimens are in good agreement with those obtained on precracked specimens.

The close correlation between c and c_0 justifies the calculation of γ_p from the fracture stress of uncracked specimens using the slow crack size, c, as the critical dimension. Since all the slow cracks had a curved front being either circular, elliptical or semi-circular, fig. 7, the Sack equation

$$\sigma_F = \sqrt{\frac{E\pi\gamma_p}{2c(1-\nu^2)}}$$

was used. The fact that a central crack of diameter $2c$ is not quite equivalent to an edge crack of radius c was neglected. The calculated

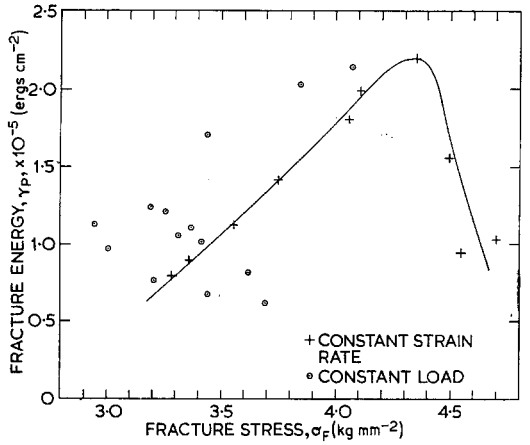

Figure 9 Variation of fracture energy with fracture stress for constant strain rate and constant load conditions calculated from c_0.

values of γ_p are shown in fig. 9. The constant strain rate results are recorded in terms of the fracture stress obtained for that strain rate to enable comparison with the constant load results. It can be seen that (*a*) γ_p is lower in these tests than in the corresponding tests on precracked specimens, and (*b*) γ_p varies with strain rate or applied load.

The results in fig. 9 are rather scattered for constant load conditions and do not show much systematic variation of γ_p with stress. Following Kambour, γ_p may be considered to be made up of a number of energy absorbing processes;

$$\gamma_p = \gamma_E + \gamma_C + \gamma_S + \gamma_H$$

where γ_E is the elastic energy of craze deformation, γ_C the energy required to form crazed material from uncrazed material, γ_S the true surface free energy, and γ_H the surface energy for void formation within the craze. In this context it would be expected that fracture associated with thick crazes would give higher values of γ_p. The results in fig. 18 of reference [6] show that in these tests the craze is thinner at high fracture stresses in apparent contradiction with this conclusion. However, an additional factor which must be taken into consideration is the dimension and shape of the craze relative to the crack.

Using Kambour's physical interpretation γ_p will clearly depend on the rate of craze growth at instability. Suppose that the distance between the crack tip and craze tip at instability is denoted by l. It is possible to define two extremes; firstly, the craze ahead of the crack is very large, e.g. right across the specimen so that l/c_0 approaches infinity, and secondly the craze ahead of the crack is very small $l/c_0 \simeq 0$. For $l/c_0 \simeq \infty$ it is reasonable to assume that the craze will not be growing significantly at instability, whereas for $l/c_0 \simeq 0$ the craze will be growing at the same speed as the crack. Hence it is expected that γ_p will be larger for $l/c_0 \simeq 0$ since γ_C will be almost zero for $l/c_0 \simeq \infty$.

For edge nucleated fractures $l/c_0 = (M - c_0)/(c_0)$ (see fig. 7). For internally nucleated fractures l cannot be deduced directly from M and c_0 since the position of the slow growth region depends on strain rate or applied load. l must, therefore, be measured direct from the specimen surface. The variation of γ_p with l/c_0 is shown in fig. 10, which is in agreement with the theory outlined above. Thus at high values of l/c_0, γ_p is small, $l/c_0 = 12$, $\gamma_p = 0.7 \times 10^5$ ergs cm^{-2}; and at low values of l/c_0, γ_p is large, $l/c_0 = 2.0$, $\gamma_p = 2 \times 10^5$ ergs cm^{-2}. If the curve in fig. 10 is extrapolated to $l/c_0 = 0$ then $\gamma_p \simeq 3.2 \times 10^5$ ergs cm^{-2}.

For precracked specimens the crack length a_2 can be regarded as being the inherent flaw size for the particular fracture stress of the individual specimen. Thus l/c_0 for precracked specimens is equivalent to $(M - a_2)/(a_2)$ and in all cases is small compared to l/c_0 for initially uncracked specimens. Typically l/c_0 lies between 0.03 and 0.5, see tables I and II. The values of γ_p of 2.3 and 2.9×10^5 ergs cm^{-2} found for precracked specimens under different test conditions are thus in fair agreement with that expected from the prediction made from results for uncracked specimens on the basis of l/c_0.

At high values of l/c_0 the curve in fig. 10 appears to reach a limiting value of γ_p of approximately 0.7×10^5 ergs cm^{-2}.

As described previously we would expect γ_C to be approaching zero at high l/c_0 values, and thus $\gamma_p = \gamma_E$ provided $\gamma_S + \gamma_H$ is negligible [5] so that $\gamma_E \simeq 0.7 \times 10^5$ ergs cm^{-2}. In addition, the γ_E term does not appear to be strongly influenced by changes in craze thickness. Further examination of the results shows that two specimens tested at different strain rates corresponding to fracture stresses of 3.25 and 4.65 kg mm^{-2} (fig. 16 of reference [6]) had identical l/c_0 ratios of 12.0. Thus for both specimens $\gamma_p = \gamma_E = 0.7 \times 10^5$ ergs cm^{-2} even though the craze thickness for the former specimen was double that of the latter (see fig. 15 of reference [6]).

It must be concluded, therefore, that the

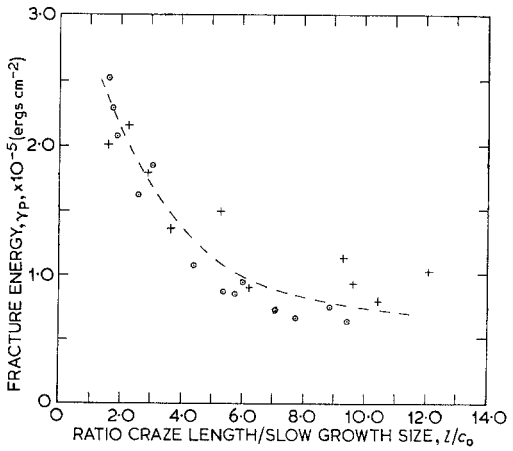

Figure 10 Variation of fracture energy with the ratio of craze length ahead of the crack tip to the inherent flaw size (l/c_0).

contribution of γ_E to γ_p is approximately constant and does not change with craze thickness. Changes in γ_p with strain rate or constant load are entirely due to changes in γ_C which are determined by the changes in the relative positions of the crack and craze.

5. Conclusions

(1) The fracture surfaces of precracked specimens consist of three regions analogous to regions A, B and C in uncracked specimens.
(2) The fracture stresses of precracked GP and SB 59 Carinex follow a Griffith type equation.
(3) The fracture energy, γ_p, of (i) GP Carinex under constant load conditions is $2.3 \pm 0.4 \times 10^5$ ergs cm^{-2} and under constant strain rate conditions is $2.9 \pm 0.7 \times 10^5$ ergs cm^{-2}. (ii) SB 59 under constant strain rate conditions is $1.5 \pm 0.5 \times 10^5$ ergs cm^{-2}.
(4) The different values of γ_p in different grades of polystyrene are determined by the craze morphology and the varying ability of the material to propagate craze material around the crack tip.
(5) Precracks are blunted during the loading and unloading experienced during cracking. Cracking whilst the specimen is loaded and testing without unloading produces a sharper crack but does not affect the measured fracture energy.
(6) In uncracked specimens, either under constant load or strain rate conditions, the slow growth region A is identified as the inherent flaw.
(7) γ_p can be calculated from c_0 in initially uncracked specimens and was found to vary with strain rate and constant load. This variation of γ_p is explained in terms of the changes in the plastic energy for craze growth at crack instability.
(8) The values of γ_p obtained in precracking experiments are consistent with the model and correspond to high craze plastic energy contributions.

References

1. J. P. BERRY, *J. Polymer Sci.* **50** (1961) 107.
2. *Idem, ibid* **50** (1961) 313.
3. *Idem, ibid* A, **1** (1963) 993.
4. E. OROWAN, Welding *J. Res. Supp.* **34** (1955) 157s.
5. R. P. KAMBOUR, *J. Polymer Sci.* A2, **4** (1966) 349.
6. J. MURRAY and D. HULL, *ibid* A2, **8** (1970) 1521.
7. *Idem, Polymer (London)* **10** (1969) 451.
8. *Idem, J. Polymer Sci.* A2, **8** (1970) 583.
9. D. HULL, *J. Mater. Sci.* **5** (1970) 357.
10. A. VAN DEN BOOGAART, in "Physical Basis of Yield and Fracture, Conference Proceedings" (Oxford, 1966) p. 167.
11. J. MURRAY and D. HULL, *J. Polymer Sci.* B, **8** (1970) 159.
12. J. G. WILLIAMS, J. C. RADON, and C. E. TURNER, *Poly. Eng. Sci.* **8** (1968) 130.
13. G. P. MARSHALL, L. E. CULVER, and J. G. WILLIAMS, *Plastics Polymers* **37** Feb. (1969) 75.
14. J. J. BENBOW and F. C. ROESLER, *Proc. Phys. Soc.* **70B** (1957) 201.
15. J. J. BENBOW, *ibid* **78** (1961) 970.
16. N. L. SVENNSON, *ibid* **77** (1961) 876.
17. J. P. BERRY, *J. Appl. Phys.* **34** (1963) 62.
18. L. J. BROUTMAN and F. J. MCGARRY, *J. Appl. Poly. Sci.* **9** (1965) 589.
19. M. HIGUCHI in "Proceedings of the First International Conference on Fracture", Sendai, Japan, **2** (1966) 1211.
20. R. W. DAVIDGE and G. TAPPIN, *J. Mater. Sci.* **3** (1968) 165.
21. H. G. TATTERSALL and G. TAPPIN, *J. Mater. Sci.* **1** (1966) 296.
22. J. G. WILLIAMS (private communication).

Received 16 April and accepted 15 May 1971